Demonstration of Fuel Hot-Spot Pressure in Excess of 50 Gbar for Direct-Drive, Layered Deuterium-Tritium Implosions on OMEGA

S. P. Regan,[1,*] V. N. Goncharov,[1] I. V. Igumenshchev,[1] T. C. Sangster,[1] R. Betti,[1,2,†] A. Bose,[1,2,†] T. R. Boehly,[1]
M. J. Bonino,[1] E. M. Campbell,[1] D. Cao,[1] T. J. B. Collins,[1] R. S. Craxton,[1] A. K. Davis,[1] J. A. Delettrez,[1] D. H. Edgell,[1]
R. Epstein,[1] C. J. Forrest,[1] J. A. Frenje,[3] D. H. Froula,[1] M. Gatu Johnson,[3] V. Yu. Glebov,[1] D. R. Harding,[1]
M. Hohenberger,[1] S. X. Hu,[1] D. Jacobs-Perkins,[1] R. Janezic,[1] M. Karasik,[4] R. L. Keck,[1] J. H. Kelly,[1] T. J. Kessler,[1]
J. P. Knauer,[1] T. Z. Kosc,[1] S. J. Loucks,[1] J. A. Marozas,[1] F. J. Marshall,[1] R. L. McCrory,[1,†] P. W. McKenty,[1]
D. D. Meyerhofer,[5] D. T. Michel,[1] J. F. Myatt,[1] S. P. Obenschain,[4] R. D. Petrasso,[3] P. B. Radha,[1] B. Rice,[1] M. J. Rosenberg,[1]
A. J. Schmitt,[4] M. J. Schmitt,[5] W. Seka,[1] W. T. Shmayda,[1] M. J. Shoup III,[1] A. Shvydky,[1] S. Skupsky,[1] A. A. Solodov,[1]
C. Stoeckl,[1] W. Theobald,[1] J. Ulreich,[1] M. D. Wittman,[1] K. M. Woo,[1,2,†] B. Yaakobi,[1] and J. D. Zuegel[1]

[1]*Laboratory for Laser Energetics, University of Rochester, Rochester, New York 14623, USA*
[2]*Fusion Science Center, University of Rochester, Rochester, New York 14623, USA*
[3]*Massachusetts Institute of Technology, Plasma Science and Fusion Center, Cambridge, Massachusetts 02139, USA*
[4]*Naval Research Laboratory, Washington, D.C. 20375, USA*
[5]*Los Alamos National Laboratory, Los Alamos, New Mexico 87545, USA*

A record fuel hot-spot pressure $P_{hs} = 56 \pm 7$ Gbar was inferred from x-ray and nuclear diagnostics for direct-drive inertial confinement fusion cryogenic, layered deuterium–tritium implosions on the 60-beam, 30-kJ, 351-nm OMEGA Laser System. When hydrodynamically scaled to the energy of the National Ignition Facility, these implosions achieved a Lawson parameter ~60% of the value required for ignition [A. Bose *et al.*, Phys. Rev. E **94**, 011201(R) (2016)], similar to indirect-drive implosions [R. Betti *et al.*, Phys. Rev. Lett. **114**, 255003 (2015)], and nearly half of the direct-drive ignition-threshold pressure. Relative to symmetric, one-dimensional simulations, the inferred hot-spot pressure is approximately 40% lower. Three-dimensional simulations suggest that low-mode distortion of the hot spot seeded by laser-drive nonuniformity and target-positioning error reduces target performance.

The spherical concentric layers of a direct-drive inertial confinement fusion (ICF) target nominally consist of a central region of a near-equimolar deuterium and tritium (DT) vapor surrounded by a cryogenic DT-fuel layer and a thin, nominally plastic (CH) ablator. The outer surface of the ablator is uniformly irradiated with multiple laser beams having a peak overlapped intensity of $<10^{15}$ watts/cm^2. The resulting laser-ablation process causes the target to accelerate and implode. As the DT-fuel layer decelerates, the initial DT vapor and the fuel mass thermally ablated from the inner surface of the ice layer are compressed and form a central hot spot, in which fusion reactions occur. ICF relies on the 3.5-MeV DT-fusion alpha particles depositing their energy in the hot spot, causing the hot-spot temperature to rise sharply and a thermonuclear burn wave to propagate out through the surrounding nearly degenerate, cold, dense DT fuel, producing significantly more energy than was used to heat and compress the fuel. Ignition is predicted to occur when the product of the temperature and areal density of the hot spot reach a minimum of 5 keV × 0.3 g/cm^2 [1–3].

Currently, the 192-beam, 351-nm, 1.8-MJ National Ignition Facility (NIF) [4] is configured for indirect-drive-ignition experiments using laser-driven hohlraums to accelerate targets via x-ray ablation. Approximately 26 kJ of thermonuclear fusion energy has been recorded on the NIF using indirect-drive ICF targets [5], where alpha heating has boosted the fusion yield by a factor of ~2.5 from that caused by the implosion system alone [6,7]. The indirect-drive NIF implosions have achieved over 60% of the Lawson parameter $P\tau$ required for ignition, where P is the pressure and τ is the confinement time [6]. Here P and τ are estimated without accounting for alpha heating to assess the pure hydrodynamic performance. The goal of achieving laboratory fusion and progress made with direct-drive ICF over the last decade motivate direct-drive implosions on NIF [8,9]. Hot-spot formation for spherically symmetric, direct-drive, DT-layered implosions is studied on the 60-beam, 30-kJ, 351-nm OMEGA Laser System [10] using hydrodynamically scaled ignition targets [11]. The radius of the target and the laser pulse duration scale with the laser energy as $E_{laser}^{1/3}$, and the laser power scales as $E_{laser}^{2/3}$.

This Letter demonstrates that a record hot-spot pressure $P_{hs} = 56 \pm 7$ Gbar was inferred for direct-drive ICF cryogenic, layered deuterium-tritium implosions on OMEGA using a suite of diagnostics including an x-ray imager having a 6-μm spatial resolution and 30-ps temporal resolution [12] and a neutron rate detector with a 40-ps

impulse response function [13]. This is nearly half of the ignition-threshold P_{hs} = 120–150 Gbar for direct-drive ICF scaled to NIF energies. These hydrodynamically scaled OMEGA implosions achieved an energy-scaled [14,15], generalized Lawson criterion without alpha heating of 60% [15], similar to indirect drive [6]. Relative to symmetric, one-dimensional (1D) simulations, the inferred P_{hs} is approximately 40% lower. Three-dimensional (3D) simulations suggest that low-mode distortion of the hot spot seeded by laser-drive nonuniformity and target-positioning error reduces the neutron rate and the inferred P_{hs}. These results indicate that higher P_{hs} could be realized by reducing the sources of the low-mode asymmetry, which is important for direct-drive ICF research to achieve an ignition-relevant P_{hs} > 100 Gbar on OMEGA, and the quest for ignition on NIF.

The P_{hs} and the conversion efficiency of the laser energy into shell kinetic energy and the hot-spot internal energy E_{hs} are critical parameters for ignition. The P_{hs} scales [11] as $P_{hs} \sim P_{abl}^{1/3} v_{imp}^{10/3}/\alpha$, where P_{abl} is the ablation pressure, v_{imp} is the implosion velocity (maximum mass-averaged shell velocity), and α is the adiabat, defined as the mass-averaged ratio of the fuel pressure to the Fermi-degenerate pressure P_{Fermi} in the dense imploding DT shell ($\alpha \equiv P/P_{Fermi}$). In the cross-beam energy transfer (CBET) process [16], non-absorbed light that is reflected or scattered from its critical surface or refracted from the underdense plasma acts as an electromagnetic seed for the stimulated Brillouin scatter of incoming (incident) light [17]. CBET has been shown to reduce the target absorption and resulting P_{abl} of direct-drive ICF targets by as much as 40% on OMEGA [16] and 60% on NIF-scale targets [18]; hydrodynamic instabilities and low-mode drive asymmetries can reduce P_{hs} and neutron rate, and the suprathermal electron generation by the two-plasma-decay instability and stimulated Raman scattering [19] can preheat the DT fuel and raise α.

A reformulation of the hot-spot temperature and areal density needed for ignition as a P_{hs} requirement is $P_{hs} > 250 \text{ Gbar}/\sqrt{E_{hs}/10 \text{ kJ}}$. Increasing laser coupling and E_{hs} reduces the P_{hs} needed for ignition. Symmetric direct-drive-ignition target designs on the 1.8-MJ, 0.35-μm NIF are predicted to couple up to 40 kJ to the hot spot, resulting in a required pressure of P_{hs} = 120 Gbar; this can be achieved in an implosion with a convergence ratio (CR) of 22 and an in-flight aspect ratio (IFAR)—defined as the shell radius divided by its thickness—of 24 when the energy coupling losses from CBET have been mitigated. Current OMEGA implosions reach E_{hs} = 0.44 kJ without any CBET mitigation. When scaled to 1.8-MJ UV energy on the NIF, these OMEGA implosions are predicted to reach $E_{hs} \approx 30$ kJ, increasing the required P_{hs} to 144 Gbar. With this E_{hs}, target designs with a CR of 25 and an IFAR of 33 are required to reach the ignition conditions. Because of the higher E_{hs} for direct-drive ICF, the ignition-relevant P_{hs} and CR are lower than the requirements for indirect-drive

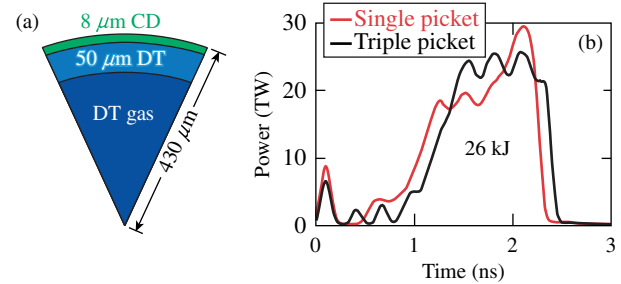FIG. 1. (a) Schematic of an OMEGA direct-drive DT-layered target. (b) The measured laser power for single- and triple-picket drives.

ICF: P_{hs} = 350–400 Gbar and CR = 30–40 [5]. An inferred P_{hs} of 226 ± 37 Gbar has been reported for NIF indirect-drive ICF implosions [7].

The hydrodynamically scaled, direct-drive, DT-layered implosions are designed with the 1D hydrodynamics code LILAC [20] to result in v_{imp} = 3.6–3.8 × 10^7 cm/s α = 2.5–4.5, CR = 15–23, and IFAR = 15–25. LILAC includes a nonlocal electron thermal conduction model [21], a CBET model [16], and a new CH first-principles equation of state [22]. The 1D simulations match the experimental observables throughout the implosion, including the scattered laser light energy and spectrum [23], shell trajectories [24], and neutron bang time [13].

The target and the laser drives used in this study are presented in Fig. 1. The target has a CD ablator with an 8-μm thickness and an outside radius R = 430 μm. Typical target-positioning errors are 5–30 μm. The DT-ice thickness was 50 ± 5 μm. The inner wall of the DT-ice layer has a 1-μm rms smoothness, and a 49:51 D:T ratio with a hydrogen (H) content less than 0.1%. The original vapor region has a 59:40 D:T ratio with ~1% of H because of isotope fractionation during layering. Most of the targets were driven with 26 kJ of incident laser energy and had two-dimensional smoothing by spectral dispersion [25] and polarization smoothing [26] on the entire pulse. Each of the
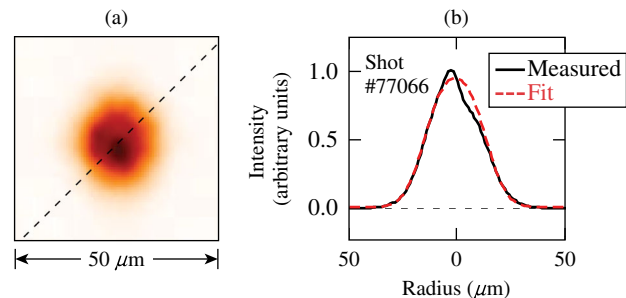

FIG. 2. (a) The measured time-resolved, x-ray image of the hot spot recorded at stagnation in the 4–8 keV photon energy range by a 16-channel Kirkpatrick-Baez microscope. (b) The measured and fitted intensity profiles taken through the center of the x-ray image along the dashed line in (a).

TABLE I.   Compilation of measured Y, $\langle T_i \rangle_n$, R_{17}, Δt_{burn}, and ρR for shots with a $P_{\mathrm{hs}} > 50$ Gbar. Quantities in parentheses are 1D simulated values. First (second) ρR measurement is diagnosed with NTOF (MRS).

Shot	Y ($\times 10^{13}$)	$\langle T_i \rangle_n$ (keV)	R_{17} (μm)	Δt_{burn} (ps)	ρR (mg/cm^2)
77064	4.2 ± 0.2 (11.0)	3.3 ± 0.25 (3.3)	22.0 ± 0.5 (21.0)	62 ± 6 (62)	211 ± 30, 191 ± 17 (216)
77066	4.1 ± 0.2 (13.1)	3.2 ± 0.25 (3.4)	21.5 ± 0.4 (22.4)	67 ± 5 (60)	221 ± 31, 193 ± 17 (211)
77068	5.3 ± 0.3 (15.0)	3.6 ± 0.25 (3.6)	22.0 ± 0.5 (19.5)	66 ± 6 (55)	211 ± 30, 194 ± 17 (245)
77070	4.0 ± 0.2 (11.8)	3.3 ± 0.25 (3.4)	20.4 ± 0.4 (19.0)	70 ± 5 (57)	220 ± 31, 229 ± 19 (243)

60 beams used a phase plate to generate a super-Gaussian far-field intensity profile on target with an order $n = 4.4 \pm 0.1$ and 95% of the laser energy encircled within a diameter of 825 ± 5 μm.

P_{hs} was inferred from x-ray and nuclear diagnostics assuming an isobaric hot spot [27]. The maximum neutron production rate is expressed as $\dot{N}_{\mathrm{max}} = n_T n_D T^2 \int_{V_{\mathrm{hs}}} dV (\langle \sigma v \rangle / T^2)$, where n_D is the number density of deuterons, n_T is the number density of tritons, T is the ion temperature, $\langle \sigma v \rangle$ is the DT fusion reactivity, and V_{hs} is the hot-spot volume. Fitting the neutron rate with a Gaussian function having a temporal width (FWHM) equal to Δt_{burn}, $\dot{N}_{\mathrm{max}}$ is related to the neutron yield Y as $\dot{N}_{\mathrm{max}} = 2Y \sqrt{\ln 2/\pi}/\Delta t_{\mathrm{burn}}$. P_{hs} is determined by combining these two expressions for $\dot{N}_{\mathrm{max}}$ assuming a 50:50 D:T mixture in the hot spot giving $P_{\mathrm{hs}} \cong \{32 Y \sqrt{\ln 2/\pi}/[\Delta t_{\mathrm{burn}} \int_{V_{\mathrm{hs}}} dV (\langle \sigma v \rangle / T^2)]\}^{1/2}$. The radius of the hot spot R_{hs} is inferred from the image of the hot spot recorded at stagnation in the 4–8 keV photon energy range with the 16-channel Kirkpatrick-Baez microscope having 6-μm spatial resolution and 30-ps temporal resolution [12]. The hot-spot image for shot 77066 is shown in Fig. 2(a), and the measured and fitted intensity profiles taken along the dashed line through the center of the image are presented in Fig. 2(b). The 17% intensity contour radius R_{17} of the gated x-ray image is related to the R_{hs} based on 1D simulations as $R_{\mathrm{hs}} = 1.06 R_{17}$. Guided by hydrocode calculations, the ion temperature is assumed to have the radial dependence as $T(r) = T_c [1 - (r/R_{\mathrm{hs}})^2 (1 - 0.15^{3/2})]^{2/3}$ with a maximum hot-spot temperature of T_c, which is constrained by the neutron-averaged ion temperature inferred from the neutron time-of-flight (NTOF) diagnostic $\langle T_i \rangle_n = [\int_{V_{\mathrm{hs}}} dV (\langle \sigma v \rangle / T) / \int_{V_{\mathrm{hs}}} dV (\langle \sigma v \rangle / T^2)]$. $\langle T_i \rangle_n$ was inferred along three lines of sight using the

technique outlined in Ref. [28], and the minimum $\langle T_i \rangle_n$ value is taken to minimize the effects of residual kinetic energy in the hot spot [29]. The time of peak neutron production and Δt_{burn} were recorded with a measurement uncertainty of ± 25 ps and $\pm 10\%$, respectively [13].

A $P_{\mathrm{hs}} = 56 \pm 7$ Gbar was inferred for shot 77066 having the following measurements: $Y = 4.1 \pm 0.2 \times 10^{13}$, $\langle T_i \rangle_n = 3.2 \pm 0.25$ keV, $R_{17} = 21.5 \pm 0.4 \mu$m, and $\Delta t_{\mathrm{burn}} = 67 \pm 5$ ps. The compressed areal density ρR is inferred from the downscattered primary DT neutrons, and was diagnosed using a NTOF detector ($\rho R_{\mathrm{NTOF}} = 221 \pm 31$ mg/cm^2) [30] and the magnetic recoil spectrometer ($\rho R_{\mathrm{MRS}} = 193 \pm 17$ mg/cm^2) [31] along different lines of sight. The 1D simulations were postprocessed to predict the x-ray and nuclear quantities of the hot spot required to infer the P_{hs}; the 1D calculated P_{hs} at bang time is 90 Gbar. A comparison of the measured target performance and the 1D simulations for implosions achieving $P_{\mathrm{hs}} > 50$ Gbar is presented in Table I. A generalized Lawson criterion without alpha heating [6,15] $\chi_{\mathrm{no}\alpha} = P\tau / P\tau_{\mathrm{ign}} = (\rho R_{\mathrm{no}\alpha})^{0.61} (0.12 Y_{\mathrm{no}\alpha}^{16} / M_{\mathrm{DT}}^{\mathrm{stag}})^{0.34}$ was calculated for shot 77066 and energy scaled $(E_{\mathrm{laser}}^{\mathrm{NIF}} / E_{\mathrm{laser}}^{\mathrm{OMEGA}})^{0.35}$ from the OMEGA laser energy $E_{\mathrm{laser}}^{\mathrm{OMEGA}} = 26$ kJ to the NIF laser energy $E_{\mathrm{laser}}^{\mathrm{NIF}} = 1.9$ MJ [14,15]. With a measured areal density of $\rho R_{\mathrm{no}\alpha} = 0.207$ g/cm^2 (average of ρR_{NTOF} and ρR_{MRS} measurements), a measured neutron yield in units of 10^{16} of $Y_{\mathrm{no}\alpha}^{16} = 4.1 \times 10^{-3}$, and a 1D calculated shocked DT mass at stagnation in units of mg of $M_{\mathrm{DT}}^{\mathrm{stag}} = 12.3 \times 10^{-3}$ mg, the $\chi_{\mathrm{no}\alpha} (E_{\mathrm{laser}}^{\mathrm{NIF}} / E_{\mathrm{laser}}^{\mathrm{OMEGA}})^{0.35} \approx 0.6$. As shown in Table II, similar performance was achieved with the single-picket and triple-picket laser drives. The direct-drive implosion performance achieved on OMEGA has been extrapolated to NIF: A detailed estimate of the fusion yield amplification due to alpha heating and the total fusion

TABLE II.   Compilation of the laser drive, α, shocked DT mass at stagnation $M_{\mathrm{DT}}^{\mathrm{stag}}$, P_{hs}(1D), P_{hs}(experiment), P_{hs}(experiment)/P_{hs}(1D), and the energy-scaled $\chi_{\mathrm{no}\alpha}$ for the shots with a $P_{\mathrm{hs}} > 50$ Gbar.

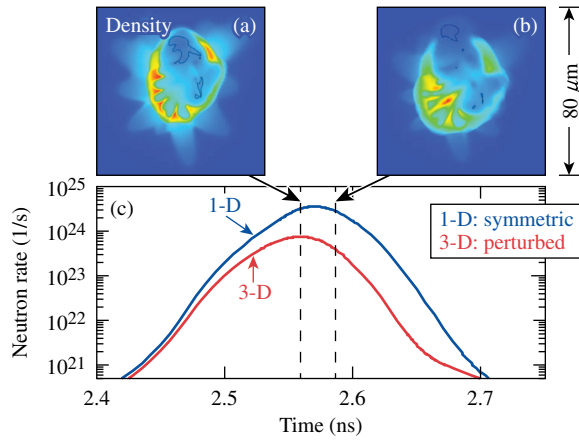| Shot	Laser drive	α	$M_{\mathrm{DT}}^{\mathrm{stag}}$ (mg)	P_{hs}(1D) (Gbar)	P_{hs}(experiment) (Gbar)	P_{hs}(experiment)/P_{hs}(1D)	$\chi_{\mathrm{no}\alpha}(E_{\mathrm{laser}}^{\mathrm{NIF}}/E_{\mathrm{laser}}^{\mathrm{OMEGA}})^{0.35}$
77064	triple picket	3.7	0.0116	91	54 ± 7	59%	0.59
77066	triple picket	3.2	0.0123	90	56 ± 7	62%	0.58
77068	single picket	3.2	0.0112	119	56 ± 7	47%	0.64
77070	single picket	3.6	0.0107	110	56 ± 7	51%	0.63

FIG. 3. ASTER simulations of the hot spot near stagnation. (a) Mass-density contour taken at earlier time, (b) mass-density contour taken at later time, and (c) 3D calculated neutron rate relative to the calculated neutron rate for a spherically symmetric implosion (1D).

yield are presented in Ref. [15] for a NIF direct-drive ignition target.

Three-dimensional hydrodynamics simulations from the code ASTER [32] are used as a guide to determine possible sources of target performance degradation. When laser irradiation nonuniformity on target caused by 15% rms beam-to-beam laser power imbalance, 20-μm target offset, and 10-μm rms beam-to-beam laser-beam mispointing are included in the ASTER simulations, the low-mode distortion of the hot spot is predicted to rupture the shell before peak compression is reached [see Figs. 3(a) and 3(b)]. This reduces the compression leading to a lower neutron production rate and lower P_{hs}. The effects of the 3D perturbations on the neutron rate can be seen in Fig. 3(c) by comparing the 3D curve with the 1D curve, corresponding to a spherically symmetric 3D implosion. The initial slope of the neutron rate is the similar for both cases until the 3D case deviates from the 1D case prior to the peak for a spherically symmetric implosion (1D bang time). The 3D perturbations cause the peak neutron rate to
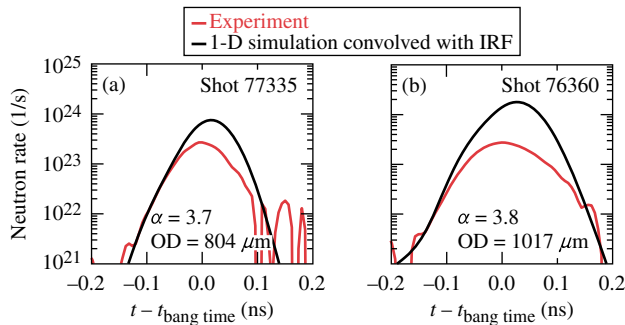
occur approximately 20 ps earlier, with a peak neutron rate that is lower than the 1D case. However, the simulated burnwidth (FWHM) is similar for 1D and 3D cases even though the neutron rate for the 3D case deviates from the 1D case [see Fig. 3(c)]. The ratio of the yield for the 3D simulation to the 1D simulation is 20% and the ratio of the P_{hs} for the 3D simulation to the 1D simulation is 50%. The $\langle T_i \rangle_n$ for the 3D and 1D simulations are similar at 2.90 keV and 3.04 keV, respectively. As can be seen in Table I, $\langle T_i \rangle_n$, R_{17}, and Δt_{burn} are close to the 1D simulated values, while the measured Y is 31%–38% of the 1D prediction, and the inferred P_{hs} is about half of the 1D simulated value (see Table II). These observations are consistent with the trends from the symmetric and perturbed 3D simulations (see Fig. 3) showing the low-mode distortion of the hot spot rupturing the shell around stagnation and limiting the compression and density of the hot spot.

A comparison of the measured neutron rate with the 1D simulation is presented in Figs. 4(a) and 4(b) for $\alpha \sim 3.7$ implosions having 804-μm and 1017-μm initial target outside diameters, respectively. The larger target is driven with 29 kJ of laser energy. The timing of the neutron rate is adjusted within the timing error (25 ps) of the neutron temporal diagnostic to match the slope of the rising edge of the neutron rate with the 1D simulation. The deviation of the measured neutron rate from the 1D simulated neutron rate is more pronounced for the larger target than the smaller one (see Fig. 4). A comparison of the measured and 1D simulated neutron rates for the smaller and larger targets shows the initial measured slope of the neutron rate is more like the 1D simulation for the smaller target and the ratio of the measured peak neutron rate to the 1D value is twice as high for the smaller target (0.36 vs 0.15). The low-mode distortion of the hot spot is expected to be more pronounced for the larger targets, since the calculated low-mode drive nonuniformity is higher for the larger target due to less beam overlap. The larger downward excursion of the measured neutron rate from the simulated one for the
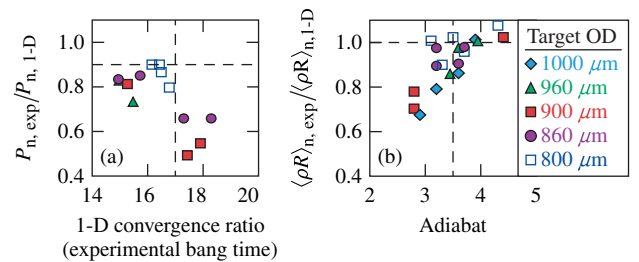

FIG. 4. Measured and 1D simulated neutron rates for $\alpha =$ 3.7–3.8 implosions having an initial target outside diameter (OD) of (a) 804 μm and (b) 1017 μm.

FIG. 5. (a) The ratio of measured P_{hs} to 1D simulated P_{hs} averaged over the measured neutron rate ($P_{n,\mathrm{exp}}/P_{n,\mathrm{1D}}$) versus the 1D simulated convergence ratio calculated at the experimental neutron bang time and (b) the ratio of measured ρR to 1D ρR averaged over the measured neutron rate ($\langle \rho R \rangle_{n,\mathrm{exp}}/\langle \rho R \rangle_{n,\mathrm{1D}}$) for targets having target outside diameters (ODs) ranging from 800 to 1000 μm versus the calculated shell adiabat.

larger target compared to the smaller target is attributed to the higher low-mode drive nonuniformity.

When the earlier peaking of the measured neutron rate relative to the 1D simulated rate is taken into account the 1-D simulations for implosions with a CR < 17 and $\alpha > 3.5$ are in closer agreement with the experimental values of P_{hs} and the compressed areal density. The ratio of the P_{hs} inferred from the experiment with the 1D simulated P_{hs} averaged over the measured neutron rate is compared to the 1D convergence ratio in Fig. 5(a), and shown to reach 90% of the 1D value for CR < 17. This behavior is attributed to a higher level of low-mode distortion of the hot spot for $\alpha > 3.5$ implosions having CR > 17. The measured areal density compared to the 1D simulated areal density averaged over the measured neutron rate is presented in Fig. 5(b), and is shown to reach the 1D value for $\alpha > 3.5$. The degraded performance for the lower-adiabat ($\alpha < 3.5$) implosions is attributed to high-mode perturbations caused by laser imprint and mass modulations in the target.

[*]Corresponding author.
sreg@lle.rochester.edu
[†]Also at Departments of Mechanical Engineering and Physics & Astronomy, University of Rochester, Rochester, New York 14623, USA.

[1] J. D. Lindl, P. Amendt, R. L. Berger, S. G. Glendinning, S. H. Glenzer, S. W. Haan, R. L. Kauffman, O. L. Landen, and L. J. Suter, Phys. Plasmas **11**, 339 (2004).
[2] S. Atzeni and J. Meyer-ter-Vehn, *The Physics of Inertial Fusion: Beam Plasma Interaction, Hydrodynamics, Hot Dense Matter*, International Series of Monographs on Physics (Clarendon Press, Oxford, England, 2004).
[3] R. Betti, K. Anderson, V. N. Goncharov, R. L. McCrory, D. D. Meyerhofer, S. Skupsky, and R. P. J. Town, Phys. Plasmas **9**, 2277 (2002).
[4] E. M. Campbell and W. J. Hogan, Plasma Phys. Controlled Fusion **41**, B39 (1999).
[5] O. A. Hurricane et al., Nature (London) **506**, 343 (2014).
[6] R. Betti, A. R. Christopherson, B. K. Spears, R. Nora, A. Bose, J. Howard, K. M. Woo, M. J. Edwards, and J. Sanz, Phys. Rev. Lett. **114**, 255003 (2015).
[7] T. Döppner et al., Phys. Rev. Lett. **115**, 055001 (2015).
[8] T. J. B. Collins et al., Phys. Plasmas **19**, 056308 (2012).
[9] V. N. Goncharov et al., Phys. Rev. Lett. **104**, 165001 (2010).
[10] T. R. Boehly et al., Opt. Commun. **133**, 495 (1997).
[11] V. N. Goncharov et al., Phys. Plasmas **21**, 056315 (2014).
[12] F. J. Marshall, Rev. Sci. Instrum. **83**, 10E518 (2012).
[13] C. Stoeckl et al., Rev. Sci. Instrum. **87**, 053501 (2016).
[14] R. Nora et al., Phys. Plasmas **21**, 056316 (2014).
[15] A. Bose et al., Phys. Rev. E **94**, 011201(R) (2016).
[16] I. V. Igumenshchev, D. H. Edgell, V. N. Goncharov, J. A. Delettrez, A. V. Maximov, J. F. Myatt, W. Seka, A. Shvydky, S. Skupsky, and C. Stoeckl, Phys. Plasmas **17**, 122708 (2010); **19**, 056314 (2012); D. H. Froula et al., Phys. Rev. Lett. **108**, 125003 (2012).
[17] C. J. Randall and J. R. Albritton, Phys. Fluids **24**, 1474 (1981).
[18] P. B. Radha et al., Phys. Plasmas **23**, 056305 (2016).
[19] W. L. Kruer, in *The Physics of Laser Plasma Interactions*, edited by D. Pines, Frontiers in Physics Vol. 73 (Addison-Wesley, Redwood City, CA, 1988).
[20] J. Delettrez, R. Epstein, M. C. Richardson, P. A. Jaanimagi, and B. L. Henke, Phys. Rev. A **36**, 3926 (1987).
[21] V. N. Goncharov et al., Phys. Plasmas **15**, 056310 (2008).
[22] S. X. Hu, L. A. Collins, V. N. Goncharov, J. D. Kress, R. L. McCrory, and S. Skupsky, Phys. Rev. E **92**, 043104 (2015).
[23] W. Seka et al., Phys. Plasmas **15**, 056312 (2008).
[24] D. T. Michel, A. K. Davis, V. N. Goncharov, T. C. Sangster, S. X. Hu, I. V. Igumenshchev, D. D. Meyerhofer, W. Seka, and D. H. Froula, Phys. Rev. Lett. **114**, 155002 (2015).
[25] S. Skupsky, R. W. Short, T. Kessler, R. S. Craxton, S. Letzring, and J. M. Soures, J. Appl. Phys. **66**, 3456 (1989); S. P. Regan et al., J. Opt. Soc. Am. B **22**, 998 (2005).
[26] T. R. Boehly, V. A. Smalyuk, D. D. Meyerhofer, J. P. Knauer, D. K. Bradley, R. S. Craxton, M. J. Guardalben, S. Skupsky, and T. J. Kessler, J. Appl. Phys. **85**, 3444 (1999).
[27] C. Cerjan, P. T. Springer, and S. M. Sepke, Phys. Plasmas **20**, 056319 (2013); R. Betti, P. Y. Chang, B. K. Spears, K. S. Anderson, J. Edwards, M. Fatenejad, J. D. Lindl, R. L. McCrory, R. Nora, and D. Shvarts, Phys. Plasmas **17**, 058102 (2010).
[28] T. J. Murphy, R. E. Chrien, and K. A. Klare, Rev. Sci. Instrum. **68**, 610 (1997).
[29] T. J. Murphy, Phys. Plasmas **21**, 072701 (2014).
[30] C. J. Forrest et al., Rev. Sci. Instrum. **83**, 10D919 (2012).
[31] J. A. Frenje et al., Phys. Plasmas **17**, 056311 (2010).
[32] I. V. Igumenshchev et al., Phys. Plasmas **23**, 052702 (2016).